RSC Advances

PAPER

View Article Online
View Journal | View Issue

Check for updates

Cite this: *RSC Adv.*, 2020, **10**, 9512

Metal oxide QD based ultrasensitive microsphere fluorescent sensor for copper, chromium and iron ions in water†

Md. Motiar R. Khan,‡[a] Tapas Mitra‡[a] and Dibakar Sahoo *[b]

Herein we developed a rapid, cheap, and water-soluble ultra-sensitive ZnO quantum dot (QD) based metal sensor for detecting different hazardous metal ions up to the picomolar range in water. Various spectroscopic and microscopic techniques confirmed the formation of 2.15 ± 0.46 μm of ZnO QD conjugated CMC microspheres (ZCM microspheres) which contain 5.5 ± 0.5 nm fluorescent zinc oxide (ZnO) QDs. Our system, as a promising sensor, exhibited excellent photostability and affinity towards various heavy metal ions. The detection limits were calculated to be 16 pM for Cu^{2+} and 0.18 nM for Cr^{6+} ions which are better than previously reported values. The simple fluorescence 'turn off' property of our ZCM microsphere sensor system can serve a two-in-one purpose by not only detecting the heavy metals but also quantifying them. Nonetheless, pattern recognition for different heavy metals helped us to detect and identify multiple heavy metal ions. Finally, their practical applications on real samples also demonstrated that the ZCM sensor can be effectively utilized for detection of Cr^{6+}, Fe^{3+}, Cu^{2+} present in the real water samples. This study may inspire future research and design of target fluorescent metal oxide QDs with specific functions.

Received 28th November 2019
Accepted 21st February 2020

DOI: 10.1039/c9ra09985a

rsc.li/rsc-advances

Open Access Article. Published on 05 March 2020. Downloaded on 12/6/2025 11:34:42 AM.
This article is licensed under a Creative Commons Attribution-NonCommercial 3.0 Unported Licence.

1. Introduction

Nowadays, fast industrialization and excessive use of enduring pesticides are causing a great deal of environmental pollution. As a result of this our natural drinking water sources are contaminated and that holds a serious threat to human and animal health. One of the leading causes of water pollution is metal ions. Thus at present, the detection and quantification of heavy metal ions is an active area of research due to their fundamental roles in a vast range of biological, chemical and environmental processes.[1,2] In fact, development of novel methods based on quantum dots (QDs) for sensing metal ions has experienced significant growth during the last decade.[3–7] Here in our study we have targeted 7 metal ions: lead, chromium, mercury, iron, copper, nickel, magnesium. Among the heavy metal ions lead (Pb^{2+}), chromium (Cr^{6+}), and mercury (Hg^{2+}) have been paid much attention as they are potentially toxic to the environment and human health.[8–12] The maximum contamination level (MCL) of Pb, Cr, and Hg in drinking water is 0.015, 0.1 and 0.001 mg L^{-1} respectively according to the report of the United States Environmental Protection Agency.[13] There are also some other heavy metal ions like nickel (Ni^{2+}), iron (Fe^{3+}), and copper (Cu^{2+}) which are essential for body but required in small amounts. An excessive amount of these metals can be dangerous to human health.[14,15]

Therefore, to develop simple, yet sensitive, reliable techniques for the detection and quantification of single or multiple heavy metal ions in water is very much essential for the environment and human health. Conventional methodologies for heavy metal analysis such as atomic absorption spectroscopy,[16] mass spectroscopy,[17] atomic emission spectroscopy[18] *etc.* are either time consuming or expensive as they rely on sophisticated equipment or complex experimental procedures. There are different electro-chemical techniques which have also been commonly used to detect metal ions present in biological and environmental specimens.[19–21] Among them voltammetry and potentiometric techniques are the most reported for the heavy metal detection.[22,23] However long-term stability, selectivity, compatibility with aqueous environments remains a significant challenge for measuring these heavy metals by this technique.

On the other hand due to simplicity and low detection limits optical detection techniques are the most convenient and promising methods.[24–27] Quantum dots (QDs) have been attracting much interest recently due to their excellent luminescent property, high quantum efficiency and photostability.[28,29] In addition, QDs have the better advantage due to their photostability, and remarkable water solubility over conventional organic fluorescence dyes. Among all the QDs, zinc oxide (ZnO) quantum dots (QDs) have been widely used for

[a]*Department of Biochemistry, University of Calcutta, Kolkata-700019, India*
[b]*School of Physics, Sambalpur University, Jyoti Vihar, Burla, Odisha 768019, India. E-mail: iamdibakar@suniv.ac.in*

† Electronic supplementary information (ESI) available: FTIR, DLS, zeta potential, microscopic image, TEM image of ZCM. See DOI: 10.1039/c9ra09985a

‡ Both authors have equal contribution.

This journal is © The Royal Society of Chemistry 2020

Open Access Article. Published on 05 March 2020. Downloaded on 12/6/2025 11:34:42 AM.
This article is licensed under a Creative Commons Attribution-NonCommercial 3.0 Unported Licence.

their unique electrical and optical properties.[30,31] However, the photoluminescence quantum yields of QDs can be degraded greatly upon exposed to oxygen, heat or light. Most of the sensors based on QDs have been used in aqueous solution and thus they have the tendency to agglomerate which leads to self-absorption and nonradiative deactivation process.[32,33] So many efforts have been made to overcome this problem.[34] Very recently, microspheres and nanospheres are increasingly being utilized as QDs-sensor platforms.[35] Microspheres not only improve the stability of QDs but also offer multicolour signals and can mask the toxicity of QDs effectively. We incorporated QDs into the microspheres which make the QDs as the most promising candidate by preventing it aggregation, guarantying good chemical properties and maintain photostability. Here, the container property of the microsphere has been used in developing fluorescent sensor array with pattern recognition ability. Although there are several researches regarding metal sensing but great challenges are the stability of sensor and sensing multiple metals ions with very low detection limit. Hence research initiatives are prerequisites in developing new fluorescent very stable sensor that are very much capable of pattern recognition of multiple metal ions in aqueous solution and having very low detection limit. In this regard, simple fluorescence titration method of different metal ions in presence of microsphere (ZCM) could be used as a pattern recognition sensor for metal ions.

In the present work, we have conjugated nontoxic fluorescent ZnO-QDs with CMC polymer and prepared microsphere using the ZnO-QDs conjugate CMC polymer (ZCM) for various heavy metal sensing. To the best of our knowledge, this is the first time where the CMC polymer is modified with ZnO-QDs for the preparation of microsphere to provide the high photostability and selectivity for heavy metal sensing. Special attention has been paid to detect different cationic metal ions like Pb^{2+}, Cr^{6+}, Hg^{2+}, Fe^{3+}, Cu^{2+}, Cd^{2+}, Ni^{2+}, Mn^{2+} with good selectivity and sensitivity. Herein, we aim to construct a fluorescent sensor platform for the pattern recognition of these multiple heavy metal ions. The fluorescence titration of different metal ions reveals that as-synthesized ZCM could function as pattern recognition sensor for several heavy metal ions. ZCM sensor will act as very stable compared to so called reported only ZnO QDs. The detection limits for different metal ions of ZCM are very low compared to those reported earlier. The idea about the use of ZCM in dual mode (sensing and quantifying) for sensing of metal ions in real water sample is also exploited here. Thus, our microsphere-based nano-biosensing system will help us to provide a potential and practical application in sensing, discriminating and quantifying the various heavy metals from real water with excellent accuracy which is very much useful for human health and environment.

2. Materials and methods

2.1 Chemicals

All chemicals used were analytical grade without further purification. Zinc acetate dihydrate ($Zn(OAc)_2 \cdot 2H_2O$), (3-aminopropyl)triethoxysilane (APTES), carboxymethyl cellulose (CMC) and potassium hydroxide (KOH) were purchased from Sigma-Aldrich, India. Solvents used were purchased locally and were of HPLC grade. Metal salts such as potassium di chromate ($K_2Cr_2O_7$), ferric chloride ($FeCl_3$), manganese chloride hydrated ($MnCl_2 \cdot 4H_2O$), mercury chloride ($HgCl_2$), lead nitrate ($Pb(NO_3)_2$), cadmium chloride monohydrated ($CdCl_2 \cdot H_2O$), potassium dichromate $K_2Cr_2O_7$, nickel chloride hydrated ($NiCl_2 \cdot 6H_2O$), magnesium chloride hydrated ($MgCl_2 \cdot 6H_2O$), copper sulphate hydrated ($CuSO_4 \cdot 5H_2O$), light liquid paraffin oil, all the solvents (HPLC grade) and all other chemicals were purchased from Mark Chemical Co, India. Stock solution (10 mM) of heavy metal ions was prepared in deionized and double distilled water and diluted to get the desired concentration of the metal ions.

2.2 Preparation of microsphere

The water-soluble fluorescent ZnO-QDs capped by APTES were prepared following the protocol of Dibakar *et al.*[36,37] Initially, 1% (w/v) carboxymethyl cellulose solution was prepared by dissolving carboxymethyl cellulose powder in double distilled water under stirring at 1500 rpm for 12 h. The fluorescent zinc oxide quantum dot capped with APTES (0.5 mg dry weight) were solubilised in 500 μL of double distilled water by ultrasonication for 30 min and added into 5 mL of carboxymethyl cellulose solution followed by incubation under stirring (1500 rpm) for 5 h at 30 °C. Now fluorescent zinc oxide quantum dot-carboxymethyl cellulose microsphere (ZCM) was prepared by water-in oil emulsion method. The ZCM solution was then added dropwise ($\sim$1 mL min^{-1}) into 25 mL of light liquid paraffin containing 100 μL of Tween-80 under stirring at 1800 rpm to form water-in-oil emulsion. Subsequently, 500 μL of 15 mM calcium chloride solution was added into the suspension and continuously stirred for another 8 h at the same speed. The obtained microsphere was then separated from the emulsion by centrifugation at 15 000 rpm for 20 min. The process of centrifugation was repeated several times for complete removal of oil. The pellet was collected and washed ethanol five times to remove residual paraffin oil, Tween-80 and unconjugated ZnO QDs (as all are solubilized in ethanol) and dried by lyophilization for further experiment.

The ZCM powder was added to deionized and double distilled water as per requirements. The aqueous dispersions of colloids thus obtained were characterized for their structural, microscopic and optical properties.

2.3 Methodology to characterize ZCM microsphere

FTIR methodology. Infra-red absorbance spectra of ZCM were recorded on Bruker ALPHA, FTIR system (typically 24 scans, resolution – 4 cm^{-1}) at wave numbers from 400 to 4000 cm^{-1}. Samples were mixed with KBr and ground to a fine power to prepare a KBr pellet containing 0.1% of ZCMs.

XRD measurement. The formation and quality of the compounds were studied using an XRD technique at room temperature with a MiniFlex powder diffractometer (Rigaku, Japan) using Cu Kα radiation (l = 1.5405 Å) at a wide range of

Open Access Article. Published on 05 March 2020. Downloaded on 12/6/2025 11:34:42 AM.
This article is licensed under a Creative Commons Attribution-NonCommercial 3.0 Unported Licence.

Bragg's angles 2θ ($20^\circ \leq 2\theta \leq 80^\circ$) with a scanning rate of 3° min^{-1}.

Estimation of percentage of cross-linking degree (TNBS assay). Degree of cross-linking was quantified using TNBS assay according to the procedure summarized by Mitra *et al.*[38] The absorbance of the resulting mixture was measured at 345 nm.

2.4 Particle size and stability measurement

The diameter of the ZCMs has been determined by optical microscopy (Olympus), TEM (JEOL JEM 2100 HR with EELS TEM (JEOL, Japan) operated at 200 kV) and dynamic light scattering method and the zeta potential of the same materials has been determined by electrophoretic light scattering using a DLS instrument (Malvern Nano-ZS, ZEN 3600). For microscopic analysis, samples were prepared by drop casting the suspension of samples on a glass slide (optical) or on a copper grid (TEM) and dried naturally. For particle size and zeta potential measurement, sample volume taken were 40 μL and 1 mL respectively.

2.5 Steady state measurement

For measuring absorption and fluorescence spectra, deionized water (Millipore) was used. The absorption spectra at 300 K were recorded with a Shimadzu spectrophotometer (Model UV-2104 PC), and emission spectra were obtained with a Hitachi F-7000 fluorescence spectrophotometer. All the experiments were done in aqueous solution. Prior to the analysis, CMC, ZnO-QDs capped by APTES and ZCM were dispersed in deionized and double distilled water by ultrasonication for 30 min. The concentration of different metal ions for all the experiments are given in the figure caption. After addition of metal ions with ZCM we constantly vortex shake it for one minute followed by the steady state measurements. The equilibration time of 1 min is enough to for the system to attain equilibrium because emission spectra remain unchanged after 1 min, validated by several times discrete scanning of each system.

2.6 Time resolved measurement

Time resolved decay measurement of ZCM in presence of different metal ions were performed using time-correlated single photon counting. The IBH 5000F NanoLED equipment (Horiba Jobin Yvon, USA) was used with DataStation software. The C-dots were excited at 338 nm using a pulsed light-emitting diode (LED) with a pulse duration of 1.2 ns and 1 MHz repetition rate. The 5000 photon counts were collected in the peak channel. Emission slits with a bandpass of 16 nm were used throughout all the experiments. The sample and the scatterer were exchanged subsequently after every 10% acquisition to ensure compensation for shape and timing drifts at the time of data collection. In addition, this settlement inhibited all types of lengthy exposure of the sample to the excitation beam, by averting all probability of photodamage to the fluorophore. The fluorescence decays were collected and interpreted using DAS 6.2 software (Horiba Jobin Yvon, USA). Deconvolution of the decay curves was accomplished by using the instrument response function and interpreting it as a sum of the exponential terms.

2.7 Real sample test using river water

To check the metal sensing and quantifying ability of our as-synthesized ZCM microsphere in environmental samples, real sample test was carried out using river water collected from Hooghly river (West Bengal, India), with pre-cleaned plastic bottle. The water was then filtered by a 0.22 μM membrane (Millipore), then centrifuged for 6 min at 8000 rpm to remove the large particles and suspended soil before use. Next in the filtered river water ZCM microsphere was added (0.1 mg mL^{-1}) and solutions of different metal ions were also separately prepared using this river water as solvent. Then the different concentrations of different metal ions were spiked with ZCM microsphere. Finally, the spiked river samples were analysed using the described sensing method and recovery efficiencies was calculated.

3. Results and discussion

3.1 Characterization of synthesized ZCMs

In XRD spectrum of ZCM (ESI Fig. S1a†) broad peaks were observed in 32° (001), 34° (002), 36° (101), 47.8° (102), 56.9° (110), 63.1° (103), 68.2° (112), respectively. XRD confirms the hexagonal structure of zinc oxide in the sample. The free –COOH groups of CMC have been exchanged their proton with the free $-NH_2$ groups of APTES capped ZnO-QDs and get ionically conjugated. And to increase the stability of the ZCM microsphere, $CaCl_2$ was added to interact with the rest of the free –COOH groups of CMC. For the detection of the QD conjugated with CMC microsphere, FT-IR spectra have been recorded (ESI Fig. S1b†). N–H stretching vibration of primary amines on the outer surface of the QDs corresponds to the signals at 2926 and 1587 cm^{-1}. The asymmetric stretching vibration of C–H bond appears in the form of peak at 2866 cm^{-1} and the peak at 1003 cm^{-1} confirmed presence of Si–O–Si groups (polymerization of APTES 10 molecules). The peak at 1093 cm^{-1} is attributed to C–N bonds vibration and the peak at 1313 cm^{-1} is due to the presence of C–H bonds. The peak at 688 cm^{-1} is to in plane bending of C–C–C groups, and the signal at ~414 cm^{-1} is due the Zn–O bond.[39,40]

Results of the percentage of cross-linking degree (TNBS assay) also suggests interaction between $-NH_2$ of QDs and –COOH of CMC (ESI Scheme S1†). About 65% conjugation was quantified by TNBS assay with ZnO QDs and CMC.

The yellowish colour was observed for only ZnO QDs solution under UV radiation. The prepared ZCM microsphere solution also exhibited yellowish colour under UV radiation which is similar to prepared ZnO QD inset Fig. 1(a). This means that microsphere what we got must contain ZnO QDs. The optical properties and energy band gap analysis of pure ZnO QDs and ZCM have explored by UV-visible absorption spectroscopy. The optical absorption of ZCM microsphere has been investigated in Fig. 1(a) in the wavelength range 250–600 nm. The absorption peak for ZnO QDs (330 nm) shift towards red for ZCM

 This journal is © The Royal Society of Chemistry 2020

Open Access Article. Published on 05 March 2020. Downloaded on 12/6/2025 11:34:42 AM.
This article is licensed under a Creative Commons Attribution-NonCommercial 3.0 Unported Licence.

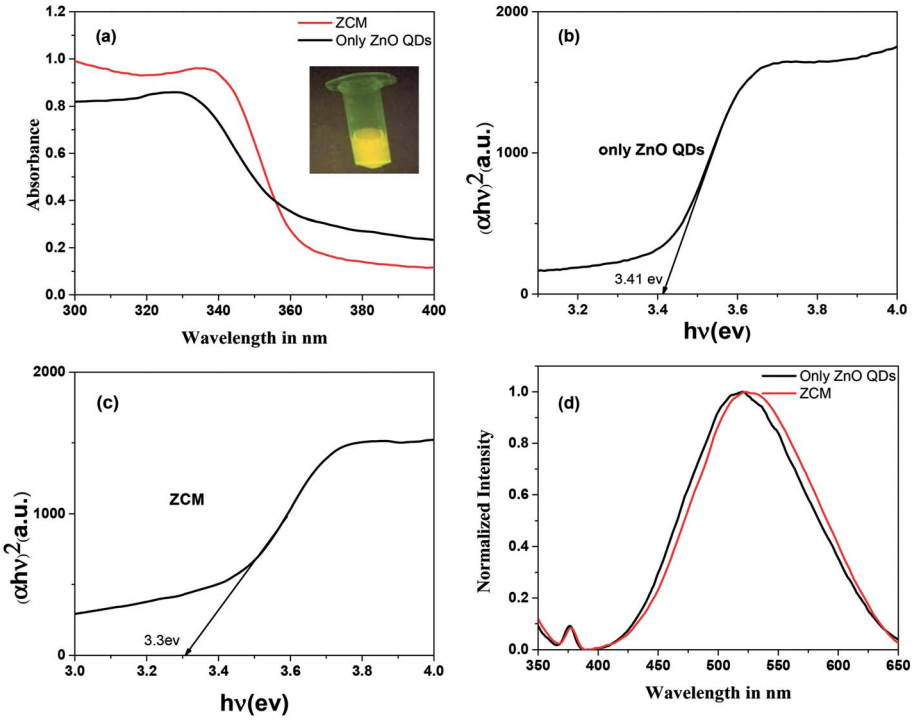

Fig. 1 (a) Absorption of QDs and ZCM microsphere (inset luminescence of ZCM microsphere under UV radiation). Optical band gap spectra of (b) QDs and (c) ZCM and (d) emission spectra of QDs and ZCM.

microsphere (337 nm) which indicate the decrease of band gap of ZnO QDs in presence of CMC. The energy band gap (E_g) is calculated by using Tauc relation,

$$\alpha h\nu = B(h\nu - E_g)^n \quad (1)$$

where α is absorption coefficient, $h\nu$ = photon energy, E_g = optical band gap, B is the constant of effective masses associated with Valance band and conduction band. $n = 1/2, 2, 3/2, 3$ for allowed direct, allowed indirect, forbidden direct and forbidden indirect transition respectively.

For allowed direct type transition the equation will be

$$\alpha h\nu = B(h\nu - E_g)^{1/2} \quad (2)$$

Band gap graphs were plotted in the linear region near the onset of $(\alpha h\nu)^2$ *versus* $h\nu$ which is shown in Fig. 1(b and c). The results show that the pure ZnO QDs has large band gap (3.41 eV) which decreases slightly when tagged with CMC. This change in band gap indicate the possibility of tagged ZnO QDs with CMC.

The fluorescence emission spectra of ZnO QDs and ZCM was shown in Fig. 1(d). In emission spectra red shift from ZnO QDs (520 nm) to ZCM microsphere (525 nm) also give the indication of conjugation of ZnO QDs with CMC. So, UV-vis and photoluminescence analysis confirm that ZCM microsphere consists of ZnO QDs conjugated with CMC.

In order to investigate the size, shape and stability of ZCM we used dynamic light scattering (DLS), zeta potential and transmission electron microscope (TEM). The DLS study shows that the hydrodynamic diameter of ZCM is 2.5–3 μm (ESI Fig. S2†) which primarily indicate that the size of microsphere sensor is in micrometre range. The value of zeta potential of CMC is −21 mV whereas only capped QDs has zeta potential −16 mV. Here negative potential of CMC induces ZnO QDs towards more negative value which in turn confirm the conjugation of QDs with CMC (ESI S2(c)†). Zeta potential is a measure of the effective electric charge on the nanoparticle surface. Particles with higher magnitude zeta potentials exhibiting increased stability due to a larger electrostatic repulsion between particles.[41] Here zeta potential value gives the moderate stability of microsphere. The average size of ZCM in fluorescence microscopic image is around 2–2.5 μm which also corroborates with DLS data (ESI S3†). The microscopic image indicates the formation of microsphere. In the TEM image several dark spot having nearly 60–70 nm size. These dark spots are mainly due to the ZnO QDs but are in aggregated form. So in TEM image we basically get the aggregated size of QDs conjugated with CMC polymer (ESI S4†).

So from TNBS assay, energy gap study, zeta potential, microscopic image and TEM image the conjugation of QDs with microsphere can be confirmed. Also above study confirm that the size of stable microsphere is nearly 2–2.5 μm having ~5.5 nm size QDs inside.

3.2 Optical sensing of metal ion

To understand the optical property of ZCM microsphere the absorption and emission spectra were recorded (Fig. 1). The fluorescence spectra were recorded after exciting at 340 nm and a broad peak at 525 nm was observed (Fig. 1(d)). The broad emission is ascribed as the excitonic transition from the surface of QDs to the defect mediated traps which is now changed for

Open Access Article. Published on 05 March 2020. Downloaded on 12/6/2025 11:34:42 AM.
This article is licensed under a Creative Commons Attribution-NonCommercial 3.0 Unported Licence.

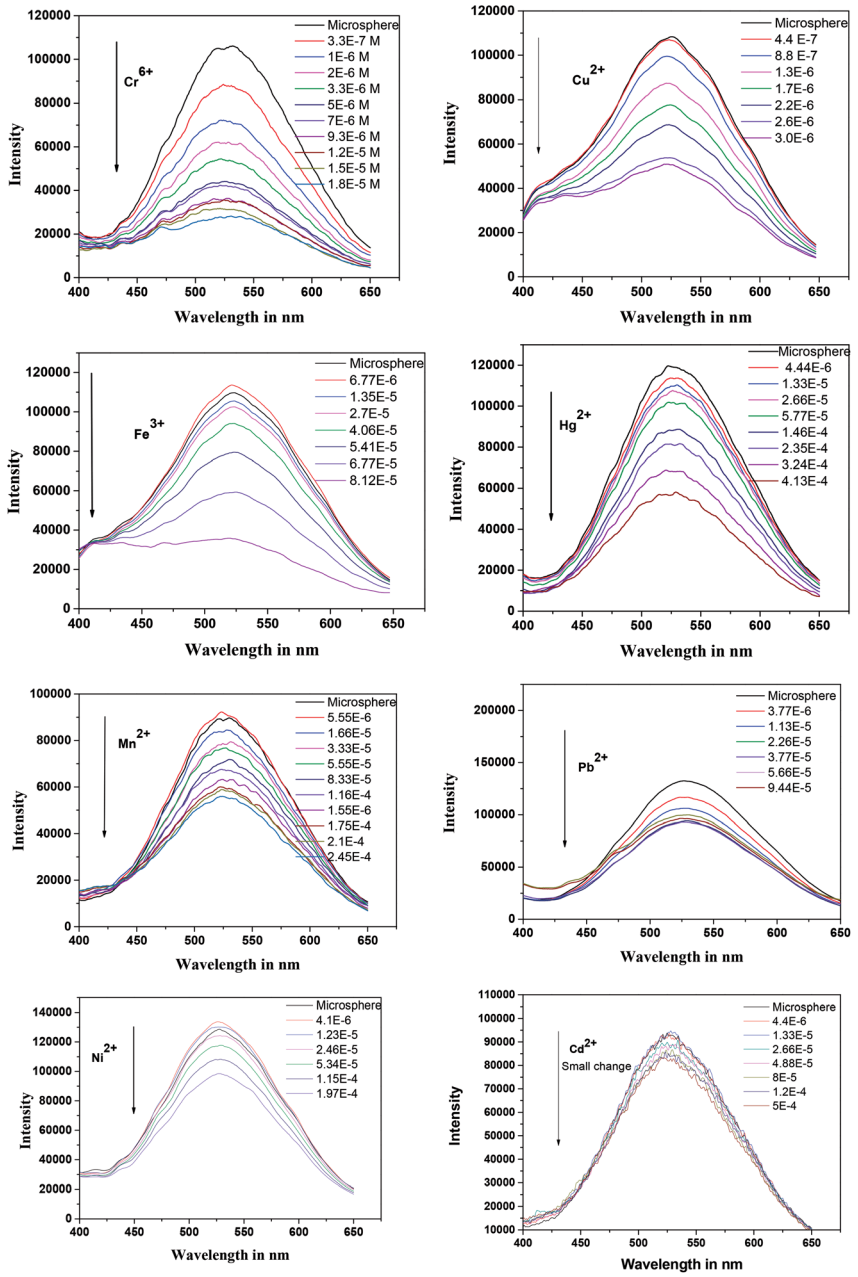

Fig. 2 Emission spectra (λ_{ex} = 340 nm) of ZCM microsphere in presence of different metal ions. The respective concentration of metal ions are shown in each graph.

CMC attachments. The environment sensitive fluorescence spectrum property of ZCM microsphere is used for our further study.

Here by using fluorescence titration method we have investigated the metal ions selectivity and sensitivity with ZCM microsphere. During the titration the concentration of ZCM microsphere was kept constant for all metal ions. The aqueous stock solution of metal ions (10 mM) in different salts were gradually titrated into the detection system. Interestingly the sensor system exhibited a different selectivity and sensitivity towards different metal ions; namely Cr^{6+}, Fe^{3+}, Cu^{2+}, Hg^{2+}, Mn^{2+}, Ni^{2+}, Pb^{2+}, Cd^{2+}. For all the system the turn off mode of ZCM microsphere was observed in fluorescence spectrum. The nature of this turn off mode is different for different metal ions (Fig. 2). This quenching of fluorescence of ZCM microsphere in presence of different metal ions added valuable information regarding the sensing property of ZCM microsphere.

The quenching mechanism of ZCM microsphere was studied and the related quenching constant were determined by using Stern–Volmer equation.[42]

$$\frac{F_0}{F} = 1 + K_{SV}[Q] \quad (3)$$

where F_0, F denotes the steady state fluorescence intensity of ZCM microsphere in absence and presence of different metal

 This journal is © The Royal Society of Chemistry 2020

Open Access Article. Published on 05 March 2020. Downloaded on 12/6/2025 11:34:42 AM.
This article is licensed under a Creative Commons Attribution-NonCommercial 3.0 Unported Licence.

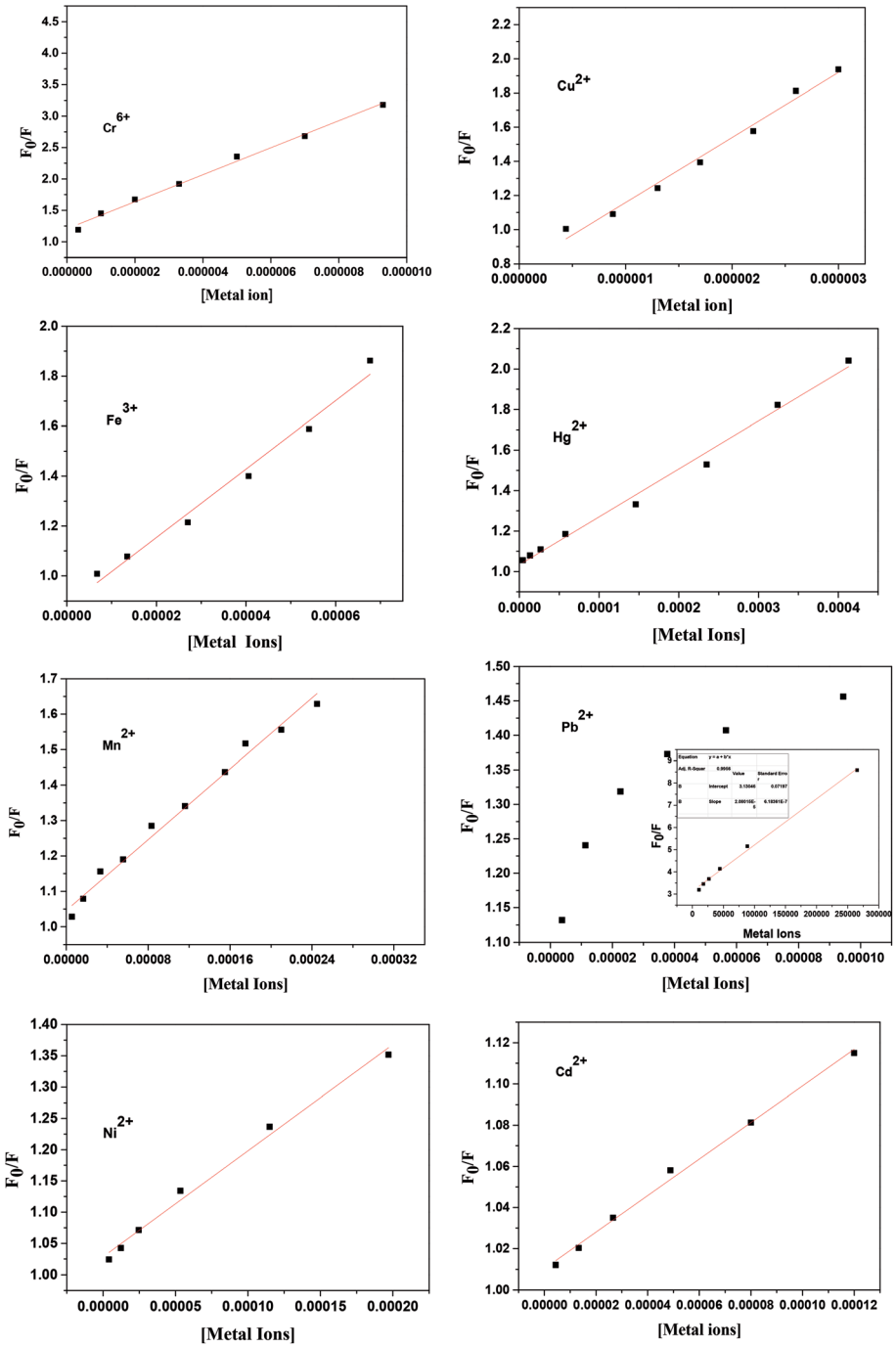

Fig. 3 Stern–Volmer (SV) plot from steady-state fluorescence emission intensity measurements of ZCM microsphere in the presence of different metal ions at 300 K. For Pb^{2+} inset shows modified SV plot.

ions respectively. K_{SV} is the Stern–Volmer quenching constant and [Q] is the concentration of metal ions.

The linear SV plot for most of the metal ions according to eqn (1) represents the involvement of only single type of quenching mechanism, either dynamic or static type.[42] Whereas for Pb^{2+} ions a downward curvature was observed (Fig. 3). This indicates that the quenching nature is dynamic but some part of ZCM microsphere is inaccessible by Pb^{2+}.[42] For Cd^{2+} the fluorescence quenching is very small meaning the interaction of ZCM microsphere with Cd^{2+} can be neglected and this metal ion cannot be reasonably detected by our ZCM microsphere system. The K_{SV} value of different metal ions are shown in Table 1. As K_{SV} value is the intrinsic property of metal ions for a particular sensor the different K_{SV} values for different metal ions easily help to discriminate them with each other's quantitatively.

3.3 Effect of pH values

In general, the pH values of probe solution have great influence on the detection of target analyte. To explore the pH

Open Access Article. Published on 05 March 2020. Downloaded on 12/6/2025 11:34:42 AM.
This article is licensed under a Creative Commons Attribution-NonCommercial 3.0 Unported Licence.

Table 1 Values of K_{SV}, K_b, n and detection limit for different metal ions

Samples	K_{SV} (10^3 L mol^{-1})	K_b (M^{-1})	N	Range (M)	R^2	Detection limit (M)
Hg^{2+}	2.36	112	0.7	$0–10^{-4}$	0.9851	7.6×10^{-9}
Cr^{6+}	215	2.9×10^3	1.2	$0–10^{-5}$	0.9934	$\mathbf{1.84 \times 10^{-10}}$
Mn^{2+}	2.46	851	0.85	$0–10^{-4}$	0.9891	8.0×10^{-9}
Cu^{2+}	385	1.2×10^{11}	2.2	$0–10^{-6}$	0.9963	$\mathbf{1.6 \times 10^{-11}}$
Fe^{3+}	13.7	2.8×10^8	2.02	$0–10^{-5}$	0.9857	$\mathbf{1.2 \times 10^{-9}}$
Ni^{2+}	1.69	141	0.7	$0–10^{-4}$	0.9910	5.3×10^{-9}
Pb^{2+}	15	29	0.6	$0–10^{-6}$	0.9942	2.1×10^{-9}
Cd^{2+}	0.88	NA	NA	NA	NA	NA

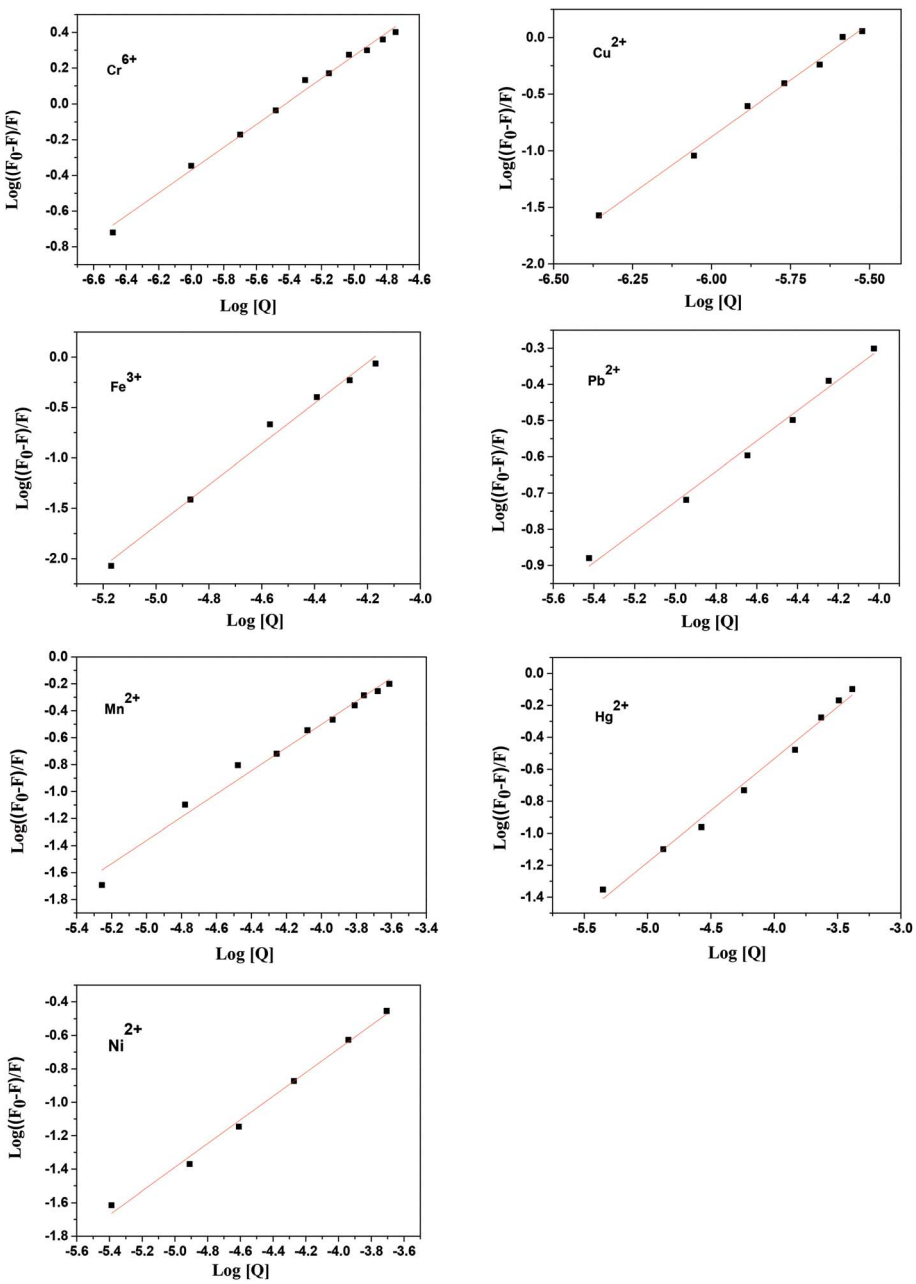

Fig. 4 Plot of log[$(F_0 - F)/F$] *vs.* log[metal ions] for the interaction of different metal ions with ZCM microsphere.

 This journal is © The Royal Society of Chemistry 2020

Open Access Article. Published on 05 March 2020. Downloaded on 12/6/2025 11:34:42 AM.
This article is licensed under a Creative Commons Attribution-NonCommercial 3.0 Unported Licence.

dependency in the detection of metal ions our ZCM has been investigated at different pH conditions. Fig. S5(a) (ESI†) infer that no appreciable alteration is observed in the fluorescence intensity of the ZCM solution inside the pH range 4–10 implying stability of ZCM under the extreme pH conditions. Its response ability towards different metal ions was also stable within the pH range from 4 to 8. Therefore, we choose the neutral aqueous solution (pH 7.02) as the analytical condition for the detection of different metal ions.

3.4 Stability test of sensor

Time scan of the fluorescence intensity was also executed at 340 nm excitation wavelength for six months to examine the stability of ZCM sensor. After 6 months the fluorescence intensity decreased to about 98% of its initial value indicating the stability of ZCM (Fig. S5(b) (ESI†)). Whereas the intensity of only ZnO QDs decreased to 94% after long time (Fig. S5(c)†). Thus, above studies signified that our ZCM acquired excellent fluorescence stability under various conditions. This advantage in stability keep ZCM as a better candidate than only ZnO QDs towards sensing.

3.5 Analysis of the binding constants and the stoichiometry of binding

The value of binding constant (K_b) that describes the binding ability of different metal ions to ZCM microsphere is helpful to understand the interaction state of the ions with ZCM microsphere. The degree of binding affinity of ZCM microsphere-ion complex can also be exploited to distinguish between the different metal ions.

To determine the binding constant (K_b) and the binding stoichiometry (n) between ZCM microsphere and respective metal ions, the following equation was employed[42]

$$\log\frac{(F_0 - F)}{F} = \log K_b + n \log[\text{ions}] \quad (4)$$

where F_0 and F are fluorescence intensity of the ZCM microsphere in absence and presence of different concentration of metal ions respectively. K_b is the binding constant and n is the stoichiometry of binding. According to eqn (4) the K_b and n values can be obtained by the plot of $\log[(F_0 - F)/F]$ *versus* log [ions] (Fig. 4).

The values of n and K_b at 300 K for the different metal ions are listed in Table 1. Among all the ions the copper and iron ions have the high affinity towards ZCM microsphere whereas nickel and mercury give very lowest affinity towards ZCM microsphere. From these hugely different values of affinity we can easily distinguished different metal ions of our interest. The structural, electrical and electrochemical differences of metal ions create different affinity of metals towards microsphere. The origin of emission of ZCM is mainly due to the recombination of electron from conduction band to deep trap electron centre.[43] The quenching mechanism of ZCM sensor in presence of different metal ions may be due to the nonradiative recombination caused by the electron transfer from ZCM to metal ions. In ZCM microsphere there are carboxyl group piping outside. With the interaction of heavy metal there are two possibility: the small ions may directly have interaction with the ZnO QDs and also the cationic group of heavy metal ions can undergo ionic interaction with the carboxyl group of ZCM microsphere. The high affinity of metal ions with carboxyl groups of CMCs on the surface of QDs results the electron transfer between ZnO QD and metal ions. This efficient electron transfer leads to the fluorescence quenching of QDs by facilitating the nonradiative recombination of excited e^-/h^+ pair. Among different metal ions the multivalent nature of Cr^{6+} and Fe^{3+} force these ions to interact and bind with free primary amine group of sensors. On the other hand, Cu^{2+} ion has large electron affinity like 118 kJ mol^{-1} than other metals also help to interact with the sensor. Moreover, the paramagnetic nature of Fe^{3+}, Cr^{6+}, Cu^{2+} produce high fluorescence quenching for ZCM microsphere sensor *via* electron transfer (Scheme 1). But for other metal ions low electron affinity compels them to interact easily with the sensor.

3.6 Time resolved fluorescence decay

Time-resolved lifetime measurements of ZCM in presence of different metal ions were performed. The fluorescence lifetime decay kinetics of the ZCM in the presence of the three metal ions were obtained which followed triple exponential fitting (ESI Fig. S6†) in every case. The lifetime of the ZCM was calculated by taking the average of three lifetime components which underwent a large decrease in its value in presence of metal ions (Table 2). The variation of average lifetime of ZCM in presence of different metal ions indicate the variation of natural

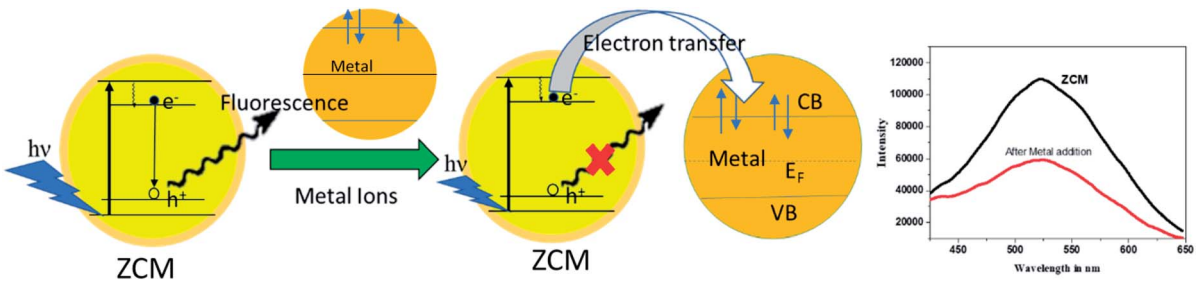

Scheme 1 Schematic representation of ZCM microsphere quenching mechanism in presence of metal ions (VB: valance band, CB: conduction band, E_F: fermi energy level).

Open Access Article. Published on 05 March 2020. Downloaded on 12/6/2025 11:34:42 AM.
This article is licensed under a Creative Commons Attribution-NonCommercial 3.0 Unported Licence.

Table 2 Fluorescence lifetime of ZCM in presence of different metal ions

Sample	τ_1 (ns)	a_1	τ_2 (ns)	a_2	τ_3 (ns)	a_3	$\langle\tau\rangle$ (ns)	χ^2
ZCM	3.32	24.32	0.22	8.94	31.3	66.74	21	1.2
ZCM + Fe^{3+}	2.99	27.7	0.19	10.53	25.82	61.77	16.8	1.19
ZCM + Cr^{6+}	3.02	32.07	0.29	10.56	25.76	57.37	15.7	1.19
ZCM + Cu^{2+}	2.55	22.95	0.04	33.58	16.65	43.47	7.8	1.11

radiative lifetime of ZCM under different metal ions environments. There should be some competition between the radiative and nonradiative excited state relaxation pathways of ZCM, therefore the variations in lifetime components imply additional non-radiative decay pathway arising from electron transfer, and the fluorescence lifetime is thus modified. The relatively shorter averaged fluorescence lifetime of ZCM in presence of Cu^{2+} can be attributed to the presence of high electron transfer activity. When the electron transfer process activity is low (for Cr^{6+}, Fe^{3+}) the non-radiative emission is less than previous one. If photoinduced electron transfer occurs, the electron transfer process quenches the radiative emission and becomes an additional nonradiative decay pathway for the excited state, the detected fluorescence signal is low and the fluorescence lifetime is altered. In these trajectories, the variations in lifetime suggest a fluctuation in the non-radiative decay rate. So the decrease of average lifetime of ZCM in presence of different metal ions indicates the electron transfer process during the interaction. Also the higher decrement of average lifetime of ZCM in presence of Cu^{2+} ions signify high activity of electron transfer and smaller decrement of average lifetime in presence of Cr^{6+}, Fe^{3+} indicate low activity of electron transfer.

3.7 Detection and quantification of heavy metal ions

The response patterns based on the quenching results were visualized by plotting the individual response of each ZCM microsphere solution upon addition of metal ions. The response was calculated as the ratio of emission intensity F/F_0. F and F_0 are the fluorescence intensity in presence and absence of metal ions. The concentration of each metal ions is kept constant (5×10^{-5} M). From Fig. 5 we can notice that among 8 metal ions 5 ions show very little change but other 3 ions *e.g.* Cu^{2+}, Cr^{6+}, Fe^{3+} have shown huge changes.

From the steady state fluorescence spectra, we observe that Cu^{2+}, Cr^{3+}, and Fe^{3+} metal ions can be detected in very low concentration by ZCM microsphere. We can also calculate the detection limit from the following formula

$$\text{Detection limit} = 3(\sigma/\text{slope}) \quad (5)$$

where σ is the standard deviation of fluorescence response and slope is determined by the gradual quenching of intensity in presence of metal ions which can get from eqn (1). A plot of fluorescence intensity at maximum as a function of metal ion concentration exhibited a good linear correlation in the concentration range of 0–100 mM for all ions excepts Cr^{6+}, Cu^{2+}, Fe^{3+} and Pb^{2+} for which the range is 0–30 μM which conclude that our sensor is very much efficient to detect various metals in low concentration (nano molar to pico molar range, Table 1). Accordingly, the ZCM microsphere sensors can be applied selectively and sensitively for detection of metal ions. Especially ZCM microsphere shows far better sensitivity towards Cu^{2+} mostly by a factor 100 and Cr^{6+} mostly by a factor of 10 as compared to those reported earlier[44–49] (Table 3).

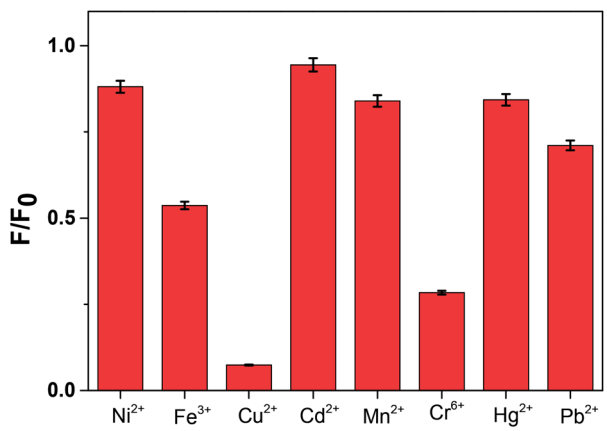

Fig. 5 Response patterns constructed based on fluorescencing quenching of ZCM microsphere by eight metal ions at constant concentration 5×10^{-5} M each. Error bars represent the standard daviation of five replicates for each measurement.

3.8 Pattern recognition ability of ZCM microsphere

To analyse the pattern recognition ability of sensor arrays by reducing the dimensionality of the data set PCA (Principal Component Analysis) has been widely utilized.[50,51] Here PCA was performed by taking the fluorescence variation of ZCM microsphere as a function of tested metal ions of different concentrations. The two-dimensional plot of PCA are shown in Fig. 6(a).

It was observed that first principle component (PCA1) carries 86.09% variance, while the second principle component (PCA2) carries 11.98% and all together these two carries about 98.08% of whole variance. From the score (Fig. 6(a)) plot it can be observed that the first two component (PCA1 and PCA2) can provide well separated cluster for most of the metal ions. From figure it can be stated that Fe^{3+} Cr^{6+}, Cu^{2+}, Pb^{2+} metal ions can be clearly detected from the cluster. Hence, our present sensor is a powerful tool to detect different heavy metals. Single sensor for the detection of large number of heavy metals can be very much useful and in high demands.

 This journal is © The Royal Society of Chemistry 2020

Open Access Article. Published on 05 March 2020. Downloaded on 12/6/2025 11:34:42 AM.
This article is licensed under a Creative Commons Attribution-NonCommercial 3.0 Unported Licence.

Table 3 Examples of some chemosensors for different metal ions detection

Metal ions	Reported sensors	Reported methods	Reported detection limits	Detection limits for ZCM microsphere
Cu^{2+}	DNAzyme	Absorption	8 nM (ref. 36)	***0.016 nM***
Cr^{6+}	Carbon paste electrode	Differential pulse cathodic stripping voltammetric	1.0 nM (ref. 32)	***0.18 nM***
Fe^{3+}	L-Cysteine (L-Cys) capped Fe_3O_4@ZnO nanoparticle	Fluorescence	3 nM (ref. 34)	1.2 nM
Hg^{2+}	Mn doped ZnSe/ZnS colloidal nanoparticles	Fluorescence	0.1 nM (ref. 35)	7.6 nM
Pb^{2+}	DNA modified T30695 sensor	Fluorescence	10 nM (ref. 30)	2.1 nM
Mn^{2+}	1,2-Bis-(2-pyren-1-ylmethylamino-ethoxy)ethane (NPEY) tagged graphene nanosheets (GNs)	Fluorescence	0.46 μM (ref. 31)	8 nM
Ni^{2+}	Fluorescein functionalized Fe_3O_4 nanoparticles	Fluorescence	0.83 nM (ref. 33)	8 nM

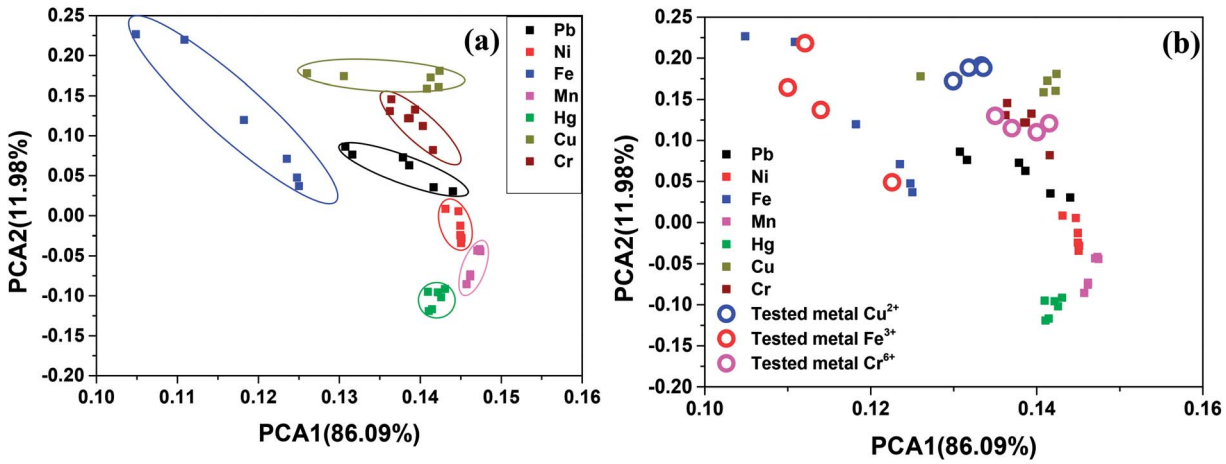

Fig. 6 (a) Two dimensional PCA score plot for the discrimination of metal ions at different concentration. (b) Two dimensional PCA score plot for determination unkown metal ions in real water (open circle Cu^{2+}, Fe^{3+} and Cr^{6+}).

3.9 Fluorescence response to mixed metal ions

As our sensor is very much sensitive for mainly three metal ions, Fe^{3+} Cr^{6+}, Cu^{2+}. The fluorescence responses of our ZCM sensor were also studied in presence of these three mixed metals ions. At first the fluorescence responses of our sensor to the mixture containing Fe^{3+} and Cr^{6+} was observed (Fig. S7†) and we found enhanced quenching for the presence of both metal ions compare to single metal ions. Same effects were shown for other combinations of metals. Secondly, we measured the fluorescence response in presence of three metals Fe^{3+} Cr^{6+}, Cu^{2+} (Fig. S8†). The co-presence of 3 metals can enhance the quenching effect of ZCM. To explore the relationship between the change in fluorescence of ZCM and the concentration of mixed metal ions, different metal ions concentration ranging from 0–30 μM (Fig. 7) was observed. Interestingly the intensity was linearly inversely proportional to the concentration of three metal ions in the range 0–2 μM (inset Fig. 7). The observation shows that ZCM not only has enough sensitivity for the detection of Fe^{3+} Cr^{6+}, Cu^{2+} but also can be used as a sensitive sensor

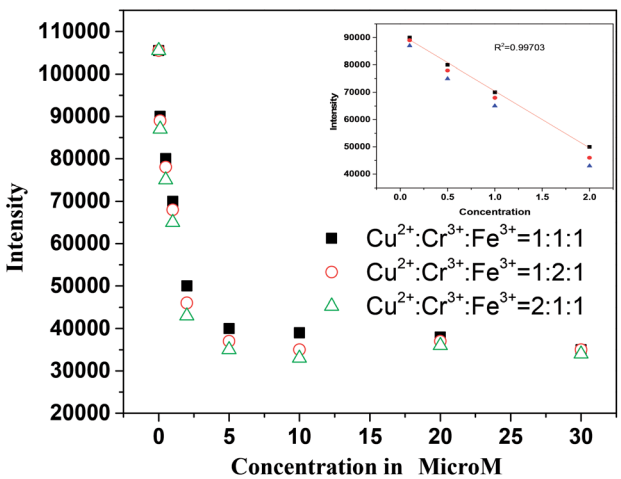

Fig. 7 Fluorescenec spectra of ZCM in presence of different concentration of mixed metal ions of different ratio.

Open Access Article. Published on 05 March 2020. Downloaded on 12/6/2025 11:34:42 AM.
This article is licensed under a Creative Commons Attribution-NonCommercial 3.0 Unported Licence.

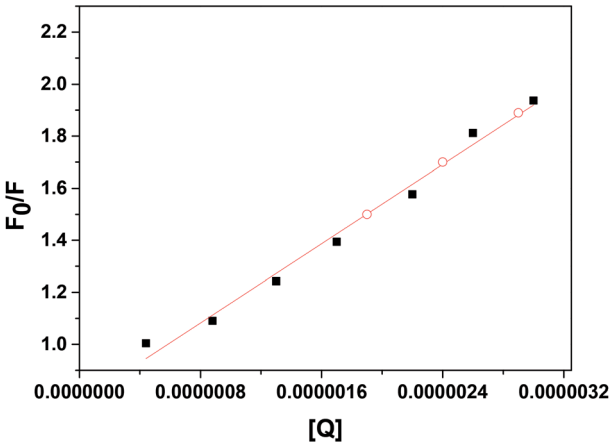

Fig. 8 Calibration curve of Cu^{2+} ions in real water. Open circles corresponds to the F_0/F value of unknown concentration of Cu^{2+} metal ions in real water.

for mixture of three heavy metal ions. Furthermore, the fluorescence intensity was also measured as a function of time which indicates instant sensing of these metal ions by our ZCM sensor (Fig. S9†).

3.10 Detection of metal ions in real water samples

To explore the potential application of the score plot for our ZCM microsphere sensor in real samples, it was used to detect Cu^{2+} and Fe^{3+} in river water. We have measured the fluorescence variation of ZCM microsphere in real water in presence of these metal ions and make a score plot along with the standard plot. From the Fig. 6(b) it is clearly indicated that in real samples score plot for our sensor give well satisfied result for detecting Fe^{3+} ions. We have done the same procedure for Cu^{2+} ions and Cr^{6+} and give the satisfactory results (Fig. 6(b)). This easy and quick determination of heavy metals in real water make the present work very interesting.

3.11 Quantification of metal ions in real water samples and recovery efficiency

Another potential application of ZCM microsphere sensor is to quantify the unknown concentrations of metal ions in real water. First, we plotted the calibration curves using fluorescence intensity variation (F_0/F) of ZCM microsphere as a function of metal ion concentration in real water. The SV plot of ZCM microsphere in real water is the calibration curves for all metal ions for ours case. The water samples were gathered from Hooghly River (West Bengal, India) and spiked with different concentrations of Fe^{3+}, Cr^{6+} and Cu^{2+} ions. Now fluorescence intensity of ZCM microsphere in real water in presence of different metal ions are measured and plotted to the calibration curve (Fig. 8). The result from this plot estimated the concentration of given metals. The results are repeated for various concentrations of three samples and it quantified the sample with good recovery efficiency (Table 4). Our sensor and used method are very much sensible to detect different metal ions as well as quantify their concentration in a very accurate way.

4. Conclusion

In summary, we have demonstrated here an effective microsphere-based fluorescence sensor of sensing different metal ions. A novel luminescence QD composite microsphere was designed to make more stable and long-lasting sensor for metals. Present sensor system exhibits different response to 7 tested metal ions. Fluorescence turn off response was adopted here to discriminate different metals ions. To our knowledge, this is the first time that microsphere-based sensor is used to detect different kind of metals. Among 7 metals Cr^{6+}, Fe^{3+} and Cu^{2+} have shown great sensitivity towards sensor system. The detection limit was estimated for Cu^{2+}, Cr^{6+} and Fe^{3+} as 16 pM, 18 nM, 1.2 nM respectively which are nearly 100, 10 and 2 times more sensitive than previously reported value. Apart from detection this sensor can quantify the metal ions within accuracy of 5% in real water. Henceforth, our sensor system can serve dual purpose: sensing and quantifying. Moreover, PCA analysis reveals that this sensor system could discriminate all the metal ions in real water very easily. Current approach demonstrates an advantageous method over other existing methods by including environment friendly fluorescent materials, simple sample preparation and measurement techniques as well as convenient data processing and straight forward pattern analysis procedure in the area of agricultural sciences in combating natural pollution and human health deterioration.

Table 4 Comparison between the measured unknown concentration of metal ions with the actual concentration in real water

Sample	Actual concentration (M)	Measured concentration (M)	Recovery efficiency (%)
Cu^{2+}	1.7×10^{-6}	$1.77 \times 10^{-6} \pm 0.25$	104.11 ± 2.4
	2.3×10^{-6}	$2.2 \times 10^{-6} \pm 0.58$	95.6 ± 1.8
	2.6×10^{-6}	$2.7 \times 10^{-6} \pm 0.91$	103.84 ± 1.9
Fe^{3+}	2×10^{-5}	$2.1 \times 10^{-5} \pm 0.11$	105 ± 2.4
	2.7×10^{-5}	$2.5 \times 10^{-5} \pm 0.43$	92.5 ± 1.92
Cr^{6+}	3.38×10^{-5}	$3.5 \times 10^{-5} \pm 0.86$	103 ± 2.1
	1.5×10^{-6}	$1.41 \times 10^{-6} \pm 0.65$	94.0 ± 1.1
	2.2×10^{-6}	$2.1 \times 10^{-6} \pm 0.77$	95 ± 2.2
	3.5×10^{-6}	$3.6 \times 10^{-6} \pm 0.27$	102 ± 1.7

This journal is © The Royal Society of Chemistry 2020

Open Access Article. Published on 05 March 2020. Downloaded on 12/6/2025 11:34:42 AM.
This article is licensed under a Creative Commons Attribution-NonCommercial 3.0 Unported Licence.

Conflicts of interest

The authors declare no competing financial interests.

Acknowledgements

Authors like to thank Prof. Anjan Kumar Dasgupta for allowing to use his lab. Authors like to thank School of Chemistry, Sambalpur University for allowing to use TCSPC. T. M. acknowledges DST, New Delhi, for financial assistance provided in the form of a SERB-National Post-Doctoral Fellowship (SERB-NPDF). D. S. thanks the University Grants Commission (UGC) for UGC-Assistant Professor position.

References

1 S. Silvi and A. Credi, Luminescent sensors based on quantum dot-molecule conjugates, *Chem. Soc. Rev.*, 2015, **44**, 4275–4289.
2 P. Wu, T. Zhao, S. Wang and X. Hou, Semiconductor quantum dots-based metal ion probes, *Nanoscale*, 2014, **6**, 43–64.
3 Y. W. Lin, C. C. Huang and H. T. Chang, *Analyst*, 2011, **136**, 863–871.
4 F. Zhang, Z. Ali, F. Amin, A. Feltz, M. Oheim and W. J. Parak, Ion and pH sensing with colloidal nanoparticles: influence of surface charge on sensing and colloidal properties, *ChemPhysChem*, 2010, **11**, 730–735.
5 F. Yarur, J. R. Macairan and R. Naccache, Ratiometric detection of heavy metal ions using fluorescent carbon dots, *Environ. Sci.: Nano*, 2019, **6**, 1121–1130.
6 M. Rana and P. Chowdhury, L-Glutathione capped CdSeS/ZnS quantum dot sensor for the detection of environmentally hazardous metal ions, *J. Lumin.*, 2019, **206**, 105–112.
7 N. De Acha, C. Elosúa, J. M. Corres and F. J. Arregui, Fluorescent sensors for the detection of heavy metal ions in aqueous media, *Sensors*, 2019, **19**, 599–633.
8 A. L. Wani, A. Ara and J. A. Usmani, Lead toxicity: a review, *Interdiscip. Toxicol.*, 2015, **8**, 55–64.
9 S. I. Hughes, S. S. R. Dasary, A. K. Singh, Z. Glenn, H. Jamison, P. C. Ray and H. Yu, Sensors and Actuators B: Chemical Sensitive and selective detection of trivalent chromium using hyper Rayleigh scattering with 5,5-dithio-bis-(2-nitrobenzoic acid)-modified gold nanoparticles, *Sens. Actuators, B*, 2013, **178**, 514–519.
10 K. M. Rice, E. M. Walker, M. Wu, C. Gillette and E. R. Blough, Environmental mercury and its toxic effects, *Journal of Preventive Medicine & Public Health*, 2014, **47**, 74–83.
11 X. H. Zhao, L. Gong, Y. Wu, X. B. Zhang and J. Xie, Cationic-perylene-G-quadruplex complex based fluorescent biosensor for label-free detection of Pb^{2+}, *Talanta*, 2016, **149**, 98–102.
12 H. Needleman, Lead Poisoning, *Annu. Rev. Med.*, 2004, **55**, 209–222.
13 United States Environmental Protection Agency, *National Primary Drinking Water Regulations*, EPA 816-F-09-004, 2009, May.
14 V. V. Shukla, Secondary Hypertension Manifests Renal Artery Stenosis and Weakened Kidney, *J. Mech. Med. Biol.*, 2011, **11**, 73–100.
15 ATSDR, *Toxic profile copper. Agency for Toxic Substances and Disease Registry*, CAS#: 7440-50-8. Copper. U.S. Public Health Service, U.S. Department of Health and Human Services, Atlanta, GA, 2004, vol. 2.
16 A. R. Ipeaiyeda and A. R. Ayoade, Flame atomic absorption spectrometric determination of heavy metals in aqueous solution and surface water preceded by co-precipitation procedure with copper(II) 8-hydroxyquinoline, *Appl. Water Sci.*, 2017, **7**, 4449–4459.
17 D. G. Bua, G. Annuario, A. Albergamo, N. Cicero and G. Dugo, Heavy metals in aromatic spices by inductively coupled plasma-mass spectrometry, *Food Addit. Contam., Part B*, 2016, **9**, 210–216.
18 S. V. Smirnova, T. O. Samarina, D. V. Ilin and I. V. Pletnev, Multielement Determination of Trace Heavy Metals in Water by Microwave-Induced Plasma Atomic Emission Spectrometry after Extraction in Unconventional Single-Salt Aqueous Biphasic System, *Anal. Chem.*, 2018, **90**, 6323–6331.
19 S. Li, C. Zhang, S. Wang, Q. Liu, H. Feng, X. Ma and J. Guo, Electrochemical microfluidics techniques for heavy metal ion detection, *Analyst*, 2018, **143**, 4230–4246.
20 Y. Meng, D. Kong, R. Wang, W. Kong, Z. Fan, Y. Huang and M. Yang, Electrochemical co-detection of heavy metals in Astragalus Membranaceus by anodic stripping voltammetry, *Int. J. Electrochem. Sci.*, 2017, **12**, 8106–8119.
21 Z. Koudelkova, T. Syrovy, P. Ambrozova, Z. Moravec, L. Kubac, D. Hynek, L. Richtera and V. Adam, Determination of zinc, cadmium, lead, copper and silver using a carbon paste electrode and a screen printed electrode modified with chromium(III) oxide, *Sensors*, 2017, **17**, 1832–1846.
22 B. J. Privett, J. H. Shin and M. H. Schoenfisch, Electrochemical sensors, *Anal. Chem.*, 2008, **80**, 4499–4517.
23 B. J. Privett, J. H. Shin and M. H. Schoenfisch, Electrochemical Sensors, *Anal. Chem.*, 2010, **82**, 4723–4741.
24 C. McDonagh, C. S. Burke and B. D. MacCraith, Optical chemical sensors, *Chem. Rev.*, 2008, **108**, 400–422.
25 D. T. Quang and J. S. Kim, Fluoro- and chromogenic chemodosimeters for heavy metal ion detection in solution and biospecimens, *Chem. Rev.*, 2010, **110**, 6280–6301.
26 A. Odobašić, I. Šestan and S. Begić, Biosensors for Determination of Heavy Metals in Waters, *Biosens. Environ. Monit.*, 2019, DOI: 10.5772/intechopen.84139.
27 L. Eddaif, A. Shaban and J. Telegdi, Sensitive detection of heavy metals ions based on the calixarene derivatives-modified piezoelectric resonators: a review, *Int. J. Environ. Anal. Chem.*, 2019, **99**, 824–853.
28 A. M. Nightingale and J. C. Demello, Improving the ensemble optical properties of InP quantum dots by indium precursor modification, *J. Mater. Chem. C*, 2016, **4**, 8454–8458.
29 D. B. Choi, S. Kim, H. C. Yoon, M. Ko, H. Yang and Y. R. Do, Color-tunable Ag-In-Zn-S quantum-dot light-emitting

Open Access Article. Published on 05 March 2020. Downloaded on 12/6/2025 11:34:42 AM.
This article is licensed under a Creative Commons Attribution-NonCommercial 3.0 Unported Licence.

devices realizing green, yellow and amber emissions, *J. Mater. Chem. C*, 2017, **5**, 953–959.

30 D. Liu, Y. Lv, M. Zhang, Y. Liu, Y. Zhu, R. Zong and Y. Zhu, Defect-related photoluminescence and photocatalytic properties of porous ZnO nanosheets, *J. Mater. Chem. A*, 2014, **2**, 15377–15388.

31 R. O. Moussodia, L. Balan and R. Schneider, Synthesis and characterization of water-soluble ZnO quantum dots prepared through PEG-siloxane coating, *New J. Chem.*, 2008, **32**, 1388–1393.

32 S. Dong, W. Guan and C. Lu, Quantum dots in organo-modified layered double hydroxide framework-improved peroxynitrous acid chemiluminescence for nitrite sensing, *Sens. Actuators, B*, 2013, **188**, 597–602.

33 C. J. Murphy, Peer Reviewed: Optical Sensing with Quantum Dots, *Anal. Chem.*, 2002, **74**, 520A–526A.

34 M. L. Chen, Y. J. He, X. W. Chen and J. H. Wang, Quantum-dot-conjugated graphene as a probe for simultaneous cancer-targeted fluorescent imaging, tracking, and monitoring drug delivery, *Bioconjugate Chem.*, 2013, **24**, 387–397.

35 Y. H. Lee, C. S. Tseng and Y. L. Wei, Fabrication and characterization of CdSe/ZnS quantum dots-doped polystyrene microspheres prepared by self-assembly, *J. Mater. Res.*, 2012, **27**, 2829–2836.

36 S. K. Arora, A. Devi, V. S. Jaswal, J. Singh, M. Kinger and V. D. Gupta, Synthesis and characterization of ZnO nanoparticles, *Orient. J. Chem.*, 2014, **30**, 1671–1679.

37 D. Sahoo, A. Mandal, T. Mitra, K. Chakraborty, M. Bardhan and A. K. Dasgupta, Nanosensing of Pesticides by Zinc Oxide Quantum Dot: An Optical and Electrochemical Approach for the Detection of Pesticides in Water, *J. Agric. Food Chem.*, 2018, **66**, 414–423.

38 T. Mitra, G. Sailakshmi, A. Gnanamani, S. T. K. Raja, T. Thiruselvi, V. M. Gowri, N. V. Selvaraj, G. Ramesh and A. B. Mandal, Preparation and characterization of a thermostable and biodegradable biopolymers using natural cross-linker, *Int. J. Biol. Macromol.*, 2011, **48**, 276–285.

39 M. Casa, M. Sarno, L. Paciello and M. Revelli, Synthesis and Characterization of Water Stable ZnO Quantum Dots Based-Sensor for Nitro-Organic Compounds, *Chem. Eng. Trans.*, 2016, **47**, 7–12.

40 Z. Wang, H. Zhang, L. Zhang, J. Yuan, S. Yan and C. Wang, Low-temperature synthesis of ZnO nanoparticles by solid-state pyrolytic reaction, *Nanotechnology*, 2003, **14**, 11–15.

41 V. R. Patel and Y. K. Agrawal, Nanosuspension: an approach to enhance solubility of drugs, *J. Adv. Pharm. Technol. Res.*, 2011, **2**, 81–88.

42 J. Lakowicz, *Principles of fluorescence spectroscopy*, 2009.

43 J. D. Ye, S. L. Gu, F. Qin, S. M. Zhu, S. M. Liu, X. Zhou, W. Liu, L. Q. Hu, R. Zhang, Y. Shi and Y. D. Zheng, Correlation between green luminescence and morphology evolution of ZnO films, *Appl. Phys. A: Mater. Sci. Process.*, 2005, **81**, 759–762.

44 X. Mao, H. Su, D. Tian, H. Li and R. Yang, Bipyrene-functionalized graphene as a 'turn-on' fluorescence sensor for manganese(II) ions in living cells, *ACS Appl. Mater. Interfaces*, 2013, **5**, 592–597.

45 D. C. Prabhakaran, J. Riotte, Y. Sivry and S. Subramanian, Electroanalytical Detection of Cr(VI) and Cr(III) Ions Using a Novel Microbial Sensor, *Electroanalysis*, 2017, **29**, 1222–1231.

46 M. T. Shah, A. Balouch and E. Alveroglu, Sensitive fluorescence detection of Ni^{2+} ions using fluorescein functionalized Fe_3O_4 nanoparticles, *J. Mater. Chem. C*, 2018, **6**, 1105–1115.

47 J. Li, Q. Wang, Z. Guo, H. Ma, Y. Zhang, B. Wang, D. Bin and Q. Wei, Highly selective fluorescent chemosensor for detection of Fe^{3+} based on Fe_3O_4@ZnO, *Sci. Rep.*, 2016, **6**, 1–8.

48 J. Ke, X. Li, Q. Zhao, Y. Hou and J. Chen, Ultrasensitive quantum dot fluorescence quenching assay for selective detection of mercury ions in drinking water, *Sci. Rep.*, 2014, **4**, 4–9.

49 W. Xu, J. Tian, Y. Luo, L. Zhu and K. Huang, A rapid and visual turn-off sensor for detecting copper(II) ion based on DNAzyme coupled with HCR-based HRP concatemers, *Sci. Rep.*, 2017, **7**, 1–10.

50 S. C. McCleskey, M. J. Griffin, S. E. Schneider, J. T. McDevitt and E. V. Anslyn, Differential receptors create patterns diagnostic for ATP and GTP, *J. Am. Chem. Soc.*, 2003, **125**, 1114–1115.

51 H. S. Hewage and E. V. Anslyn, Pattern-based recognition of thiols and metals using a single squaraine indicator, *J. Am. Chem. Soc.*, 2009, **131**, 13099–13106.

 This journal is © The Royal Society of Chemistry 2020